Journal Paper

"New Pipe Notch Detection and Location Method for Short Distances employing Ultrasonic Guided Waves"

- Acta Acustica united with Acustica-

Published: September/October 2017

Carlos Quiterio Gómez Muñoz
Ingenium Research Group, Universidad de Castilla-La Mancha
CarlosQuiterio.Gomez@uclm.es

Fausto Pedro García Márquez
Ingenium Research Group, Universidad de Castilla-La Mancha
FaustoPedro.Garcia@uclm.es

Fausto Pedro García Márquez
Ingenium Research Group, Universidad de Castilla-La Mancha
FaustoPedro.Garcia@uclm.es

Benjamin Lev
College of Business, Drexel University, Philadelphia, USA

Alfredo Arcos Jimenez
Ingenium Research Group, Universidad de Castilla-La Mancha
Alfredo.Arcos@alu.uclm.es

Cite as: Muñoz, C. Q. G., Marquez, F. P. G., Lev, B., & Arcos, A. (2017). New Pipe Notch Detection and Location Method for Short Distances employing Ultrasonic Guided Waves. Acta Acustica united with Acustica, 103(5), 772-781.

DOI: https://doi.org/10.3813/AAA.919106

ACTA ACUSTICA UNITED WITH ACUSTICA
Vol. 103 (2017) 772 – 781
DOI 10.3813/AAA.919106

New Pipe Notch Detection and Location Method for Short Distances employing Ultrasonic Guided Waves

Carlos Quiterio Gómez Muñoz[1)], Fausto Pedro García Marquez[1)], Benjamin Lev[2)], Alfredo Arcos[1)]
[1)] Ingenium Research Group, Universidad Europea de Madrid, Spain.
CarlosQuiterio.Gomez@universidadeuropea.es
[2)] Drexel University, LeBow College of Business, Philadelphia, PA USA. bl355@drexel.edu

Summary
This paper presents a novel signal processing approach that is able to automatically identify notches in pipelines in short distances. In addition, this method locates the geometric position of the notch and determines the size. The approach for fault detection and diagnosis presented look for a solution and then validates the solution by analyzing the signal which flows in the opposite direction. Micro Fiber Composite (MFC) transducers are used in an austenitic stainless steel pipeline, used in solar concentrators, in order to generate Ultrasonic Guided Waves. The main results presented in this paper can be summarized as: identification of edges or welds by multi-parametric analysis and comparison with the theoretical results predicted, notch location in the pipe by comparison of the position of echoes weighted with their amplitudes, and the flow sizing of them by using attenuation curves of the echoes when they propagate along the pipeline. This approach leads to employ only one transmitter and one receptor for notch detection, location and diagnosis. The main advantage for the industry is the double check of presence of a notch with respect to other systems, which reduces false alarms during the inspections.
PACS no. 43.35.Ae, 43.35.Yb, 43.35.Zc, 43.60.Bf, 43.60.Hj, 43.60.Qv

1. Introduction

The importance of non-destructive testing for pipelines has significantly increased in recent years due to the surge of pipelines in the gas, petrol, chemical and energy generation industries. Non-destructive testing techniques can identify structural damage at a very early stage and prevent further failures, reducing economic loses [1]. Structural health monitoring, together with advanced signal processing methods provide current status of the pipes [2]. This information leads the identification and diagnosis of the fault in a pipe and its location [3, 4], and thus, strategies can be set for predictive maintenance [5, 6, 7, 8]. In addition, these techniques can be controlled remotely, reducing the maintenance costs, downtimes, etc. [9, 10, 11, 12].

Inspection techniques using guides waves are being employed in structural monitoring techniques. This is due in large part to the drawbacks encountered in other non-destructive testing techniques, such as thermography and radiography. An example of one such drawback occurs when examining solar concentrator pipes. Thermography has a limited ability to identify internal defects if they are not outwardly manifested as temperature, and industrial radiography is dangerous for people who are close to the inspection site. Furthermore, the long range of the guided waves can inspect a greater distance than other techniques.

The inspection by guided waves consists of the excitation of an ultrasonic transducer, that generates ultrasonic waves that are propagated through the pipe [13]. The main advantage offered by this technique, compared with traditional ultrasonic methods, is the ability to inspect structures, such as plates or pipes, along several meters. This technique permits to know the state of the pipe at a specific location. In some cases, hundreds of meters can be inspected without the relocation of the transducer. Novel methodologies in signal processing are being published, such as predictive analysis online, in order to be employed in structural health monitoring and ultrasonic waves [14, 15].

The purpose of this paper is to design a novel fault detection and diagnosis (FDD) [16, 17] model using ultrasound inputs in conjunction with advanced signal processing methods [18, 19] to monitor the structural condition of austenitic stainless steel pipes [20]. This paper presents a novel signal processing approach that is able to automatically identify notches in pipelines. In addition, this method locates the geometric position of the notch and determines the size of the damage. It finds a solution and then it is validated analyzing the signal that flows by other way. This approach leads to employ only one transmitter and one receptor for fault detection, location and diagnosis.

Received 17 June 2016,
accepted 2 August 2017.

2. State of the art

Pipelines are used in long-distance transport of gas and liquid, e. g. fossil fuel. The environmental impact due to any failure of the pipes can be critical. The main defects are corrosion [21] delamination [22] and cracks [23, 24, 25], that can occur on both inner and outer surface. It is crucial to detect faults in an early state, before they grow and can traverse the thickness of the pipe, causing any failure [26].

Ultrasonic waves technique has been used in curved structures [27]. Lamb waves are guided waves that propagate in thin plate structures or shell structures [28]. The interest in Lamb waves to identify structural damage has increased in recent years [29, 30, 31, 32, 33, 34, 35]. Lamb waves have the property of propagating for long distances in plates and sheets and its application is useful for covering large areas [36].

A review on the state of the art of Lamb wave-based damage identification approaches for composite structures is done in [26]. Reference [22] presents a new Lamb wave-based delamination detection technology that allows detection of delamination in a single wave propagation path without using prior baseline data or a predetermined decision boundary. A numerical modelling and simulations of PZT-induced Lamb wave propagation in plate-like structures by using the spectral finite element method is introduced in reference [23]. A pattern recognition is employed in reference [37], where the accuracy is increased by algorithm by the reconstruction of the baseline signal. The signal processing methods found in the literature are not auto-validated.

Cylindrical Lamb waves

There are novel research studies that show the fault detection in pipes by Lamb Waves inspection [38, 39, 40]. Fault identification using Lamb waves is in an early stage of development compared with other techniques, e.g. ultrasonic scanning. Depending on the directions of propagation, guided waves in cylindrical pipes can travel in circumferential or axial direction. Gazis *et al.* studied the propagation of harmonic waves in a long elastic hollow cylinder [41, 42]. Fitch, Silk and Bainton [40, 43], applied and studied the different wave modes in hollow cylinders.

Cylindrical Lamb wave's modes are longitudinal, torsional and flexural, labelled with L, T and F respectively. The cylindrical Lamb wave's modes have two integers, $L(n, m)$, $T(n, m)$, and $F(n, m)$, $(n, m = 0, 1 \ldots)$: $n = 0$ indicates that the pipe is axially symmetric, being the case in most applications; m indicates the mode number, e.g. $L(0, 1)$ propagates through the thickness of the pipe similar to the A_0 mode in flat plates, and $L(0, 2)$ mode propagates similar to the S_0 mode in plates. $L(0, 1)$ and $L(0, 2)$ are the most appropriate modes for damage identification because of their axisymmetric properties facilitate the inspection along the circumference of the pipe.

The guided wave mode selection and the excitation frequency depend on the type of defect. In the references [44, 45], it is suggested that the S_0 is more sensitive to detect cracks located in the centre of the thickness. However, the S_1 is more efficiency for detecting cracks close to the surfaces. The calculation of the reflection factor for a longitudinal mode showed that close to the first cutoff frequency there were many mode conversion, and the results found were not clear enough. The problem could not be analyzed employing lower-frequency, i.e. it did not present a clear sensitivity to detect small cracks. The results are good when the shear horizontal mode is used. The shear horizontal circumferential guided waves were used for detecting the crack.

Wang *et al.* considered the characterization of defects and analysed the reflections of edge echoes and defect echoes [46]. It was generated as an artificial notch as defect in each pipe, setting the axial and circumferential extent and radial depth. The three parameters were increasing by a milling machine. The edges were of the front and back of defect, being the pipe length 2030 mm. The signal generated from the defect reflection involved overlapping signals as result of the reflections at different edges of the defect. The signals were coincident when they were originated from the front edge of the defect at the two axial extents. The signal from the back edge of the defect presented irregular change. The overlapping of both signals analyzed individually. The reflection problem was divided into several small problems associated to edge reflection. Two edge signals provided more independent and correlated information sources of defect. It was detected from the front-edge signal by extending the axial extent of the defect. The back-edge signal, embedded in the overall reflection at different axial extents, could be extracted by subtracting the reference from each reflection signal.

Different methodologies to detect and locate cracks in pipelines by the Time of Flight (ToF) and the analysis of the Lamb waves propagation have been done. Tua *et al.* used it for the detection of cracks in an aluminium plates with welds and pipes [46, 47]. The novel approach presented in this paper identifies, determines the size and locates defects in pipelines for short distances. The approach finds a solution and then it is validated analyzing the signal that flows by other way, presenting a novelty regarding to the state of the art.

3. Case study

The novel method for fault detection and diagnosis has been applied in a case study to validate it. The notch has been induced between two transducers. However, it would be possible to use many actuators to provide complete coverage of the pipe [46].

The distance between transducers and the edges, together with the propagation velocity, will provide the location of the notch in case there is.

Macro fiber composite transducers

The macro fiber composites, developed at NASA's Langley Research Centre, are composed of piezoceramic fibers

Table I. Physical properties of 316L austenitic stainless steel.

Parameters	Quantity
Nomenclature	316L (AISI) / 1.4404 (DIN)
Density	7.9 kg/dm^3
Young	$200 \cdot 10^3$ MPa
Poisson ratio	0.3
Dimensions	Diameter: 73 mm
	Thickness: 3.05 mm
	Length: 1.95 m

that are incorporated into an epoxy resin [48, 49]. The piezoceramic fibers are unidirectionally aligned and embedded between two sets of inter-digitated electrodes. It can be adapted to curved shell structures, and, consequently, it fits properly in pipes. Transducers are identical and they can reverse their roles.

The transducers have been arranged on the pipe to generate the modes $L(0,1)$ and $L(0,2)$ (Figure 1).

The type of MFC transducer employed in this paper were M2814-P1 (Smart Material Corp.). This type of MFC, which is available in d33 operational mode, actuates and senses along the length of the MFC patch [50].

Properties of stainless steel pipe

The 316L austenitic stainless steel is used in the chemical and petrochemical industries. It is within the Cr-Ni-Mo group designed for increased resistance to pitting corrosion. The material used is considered isotropic. The physical properties of this material are shown in Table I.

The velocities of the Lamb waves are dependent on wave frequency and the thickness of the pipe, known as dispersion. The dispersion of these waves can be predicted by the dispersion equations of Lamb waves [51], and the graphical solutions of the equations are the dispersion curves. Figure 2 shows the relationship with the group velocity and frequency for the pipe of 3.05 mm thick.

Experimental procedure

It was designed and developed an algorithm to detect changes in the thickness of the pipe, to locate them and to determine the size of the damage.

An experimental platform for ultrasonic inspections has been designed and developed to carry out the experiments. Figure 3 consists of a device that is capable to read and generate signals up to 4 MS/s. The device is connected to a PC for condition monitoring. The high frequency amplifier is used to enhance the signal to noise ratio. The actuator is driven by the computer and different input signals can be generated. Cylindrical Lamb waves were activated in the 316L austenitic stainless steel. Two MFC transducers were employed, one of them as actuator and the other as a sensor.

Different frequencies were analysed to identify the best frequency for this case study. Note that different excitation frequencies, geometries or materials will result in another propagation velocity. The selected frequency was 200 kHz

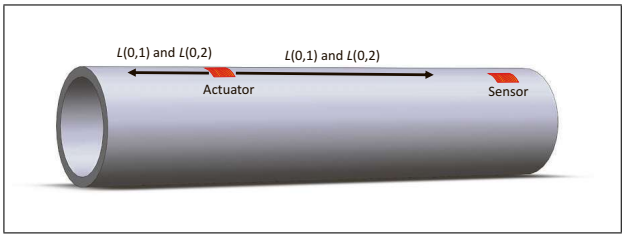

Figure 1. Longitudinal cylindrical Lamb waves in a pipe section, activated by the actuator and received by the sensor.

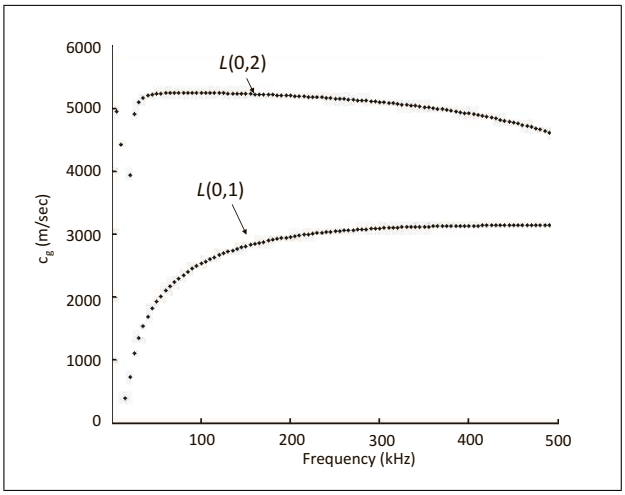

Figure 2. Dispersion curves of group velocity of 316L steel pipe. Longitudinal modes: L(0,1) and L(0,2).

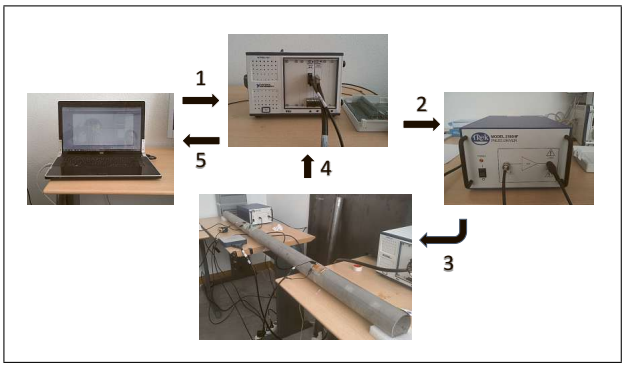

Figure 3. Experimental platform for ultrasonic inspections.

and 6 cycles pulses, according to the references [52, 53] where it is shown that a narrow bandwidth signal with a certain number of cycles can greatly prevent wave dispersion. The guided waves were collected by the sensor.

The case study consists of two scenarios; the first is to obtain reference signals of the pipe without any defect; for the second scenario is induced a fault with six different depths. The damage is a transversal cut of 2 cm long, and the increment of depth of each cut is 0.5 mm.

Figure 4 shows the location of the transducers and induced crack on the pipe.

4. Signal processing

The signal processing approach is based on system identification techniques in discrete time to estimate faults. The Hilbert Transform will be employed together with an automatic peak detection algorithm.

The method detects the peaks that correspond to echoes reflected from the edges [54]. It can be extended to other discontinuities that produce a reflection in the ultrasonic pulse, e.g. welds. This is used for the inspection of welded pipes in series, e.g. gas&oil transportation and concentrated solar plants [55, 56]. The echoes that come from the edges are discarded. The rest of echoes are analysed as feasible faults. The two echoes that come from the same feasible point are identified. The distances from the transducers to the edges and the velocity of propagation of the ultrasonic pulse are employed in the approach. The algorithm shows the exact location of the defect when the potential crack is detected, and the severity of the damage is calculated by comparison with the reference signal.

4.1. Envelope and smooth

The Hilbert Transform is employed to obtain the envelope of the filtered signal. The Hilbert transform is an approach to study the energy distribution of a Lamb wave in the time domain [57]. It is useful to obtain the energy envelope, where local features can be identified [58]. It is necessary to smooth the envelope to find events in the signal (mainly peaks). An inadequate window size could produce distortions as "saw tooth" in the signal. A good result is achieved by a Wavelet denoising filter to the low frequency decompositions (approximations) [59].

4.2. Correction method

Pattern recognition has been employed for fault detection and diagnosis. Captured Lamb waves are correlated with the reference signal for a healthy condition [52]. Damage in the structure can thus be detected and quantified by pattern recognition considering as reference the healthy state.

λ_{xy} is the correlation coefficient of two Lamb wave signals, $\boldsymbol{x}$ and $\boldsymbol{y}$. The size of the discrete signals is the same (N samples) [60, 61]. The correlation coefficient is defined by equation (1).

$$\lambda_{xy} = \frac{N\sum_{i=1}^{N} x_i y_i - \sum_{i=1}^{N} x_i \sum_{i=1}^{N} y_i}{\sqrt{N\sum_{i=1}^{N} x_i^2 - \left(\sum_{i=1}^{N} x_i\right)^2}\sqrt{N\sum_{i=1}^{N} y_i^2 - \left(\sum_{i=1}^{N} y_i\right)^2}}. \quad (1)$$

When $\lambda_{xy} = 1$ signal $\boldsymbol{x}$ is very similar to signal $\boldsymbol{y}$. If a signal is correlated with itself is called autocorrelation.

The pattern recognition approach is based on the autocorrelation of both signals, "reference" and "damaged" signals. Then the autocorrelation of the signal with damage is divided by the autocorrelation of the reference signal to emphasize the differences and to obtain the ratio curve between them.

One advantage offered by the ratio curve is that highlights the differences between two signals it attenuates the similarities between them. An example of similarity between signals are the echoes that come from the edges (present in all the cases regardless of the damage). It produces the weakening of the boundary effect.

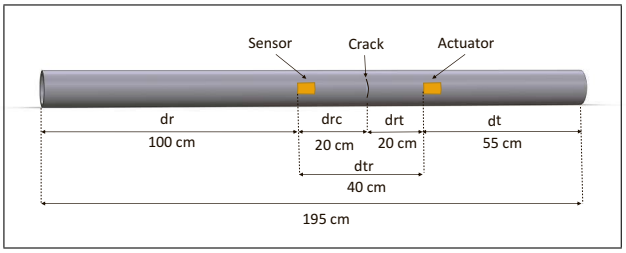

Figure 4. Location of the crack in the pipe and location of the MFCs.

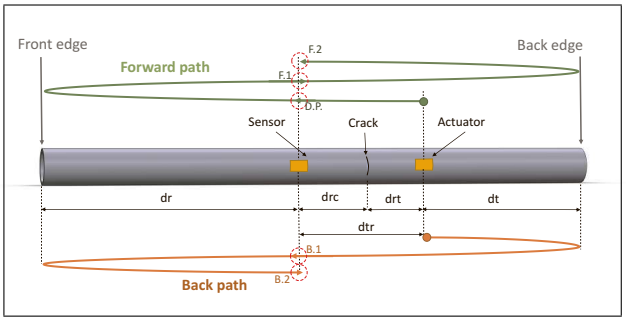

Figure 5. Two shortest paths from actuator to sensor detecting the crack.

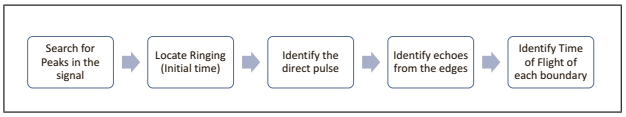

Figure 6. Identification of edges echoes algorithm.

4.3. Edges location

The novel approach firstly identifies the echoes that come from the edges of the pipe. The guided waves generated by the actuator are propagated in two directions, forward and backward. Also both modes $L(0,1)$ and $L(0,2)$ are generated in both directions. $L(0,2)$ mode is analysed and direct pulse is detected and the propagation velocity determined.

Then, two edge echoes on each path are studied. On the forward path, the first two edge echoes (F.1 and F.2) are found. In the same way, the first two reflections along the back path are detected (B.1 and B.2).

The location of the echoes that come from the edges are theoretically calculated by the travelled distance (forward and back) and the propagation velocity. They are analysed together with the experimental results, and the real echoes in the signal (peaks) that coincide with the theoretical edge echoes are identified.

The process shown in Figure 6 consists of the following steps:

- Peak searching: It is important to select the proper threshold for this purpose.

- Identify the first event that indicates the instant when the actuator is excited.
- Identify the first pulse received by the sensors of each wave mode (Direct Pulse).
- Identify echoes from the edges: The experimental ToF of each echo in the signal is obtained and compared with the theoretical ToF that they should have. The comparison sequence for identification of the edges is shown in Figure 7 [62, 63].
- The ToF of each echo is identified to calculate the distance travelled.

Vector $\boldsymbol{X}$ contains the position values of the peaks obtained experimentally, $\boldsymbol{Y}$ contains the height of the peaks of $\boldsymbol{X}$ and $\boldsymbol{X}^*$ contains the position values of the peaks obtained theoretically.

$$\begin{aligned}\boldsymbol{X}^* &= \left[x_1, \ldots, x_i, \ldots, x_n\right],\\ \boldsymbol{Y}^* &= \left[y_1, \ldots, y_i, \ldots, y_n\right],\\ \boldsymbol{X}^* &= \left[x_1^*, \ldots, x_i^*, \ldots, x_n^*\right].\end{aligned}$$

The matrix $\boldsymbol{C}$ (Equation 2) contains the difference between each value of $\boldsymbol{X}$ and each value of $\boldsymbol{X}^*$.

$$\boldsymbol{C} = \begin{bmatrix} |x_1 - x_1^*| & \cdots & |x_1 - x_j^*| & \cdots & |x_1 - x_m^*| \\ \vdots & & \vdots & & \vdots \\ |x_i - x_1^*| & \cdots & |x_i - x_j^*| & \cdots & |x_i - x_m^*| \\ \vdots & & \vdots & & \vdots \\ |x_n - x_1^*| & \cdots & |x_n - x_j^*| & \cdots & |x_n - x_m^*| \end{bmatrix}, \quad i = 1, \ldots, n, \quad j = 1, \ldots, m. \tag{2}$$

The purpose of this approach is to select the real peaks having its theoretical homologous. For each x_i, the most similar value x_j^* is chosen if the difference between them is less than the tolerance θ, else an alarm would notice that the similitude has not been found. The minimum value of the components of each column $\boldsymbol{C}_j$ is given by a particular x_i. $\boldsymbol{X}_{\text{edges}}$ is a subset of $\boldsymbol{X}$ that contains the minimum values of each column $\boldsymbol{C}_j$, i.e.

$$\begin{aligned}\boldsymbol{X}_{\text{edges}} &= \left[X_{\text{edges}_1}, \ldots, X_{\text{edges}_j}, \ldots, X_{\text{edges}_m}\right], \\ X_{\text{edges}_j} &= \chi_r, \chi_r \in \boldsymbol{X}\ \forall r, j : \\ c_{rj} &= \min(\boldsymbol{C}_j) \leftrightarrow c_{rj} < \theta,\ j = 1, 2, \ldots, m.\end{aligned} \tag{3}$$

This method detects the absolute and relative error between the value obtained and expected for each event. Figure 8 shows the edges location of the $L(0, 2)$ with a propagation velocity of 5020 m/s.

"X" markers in Figure 8 are the theoretical location of the echoes that come from the edges. The numbers 1–6 in Figure 8 and Figure 9 indicate:

1. The instant when the actuator is excited and emits the pulse.
2. The Direct Pulse (D.P.), i. e. the shorter distance between the actuator and the sensor.
3. The first reflection from the back edge (B.1).
4. The first reflection from the front edge (F.1).
5. The second reflection from the back edge (B.2).

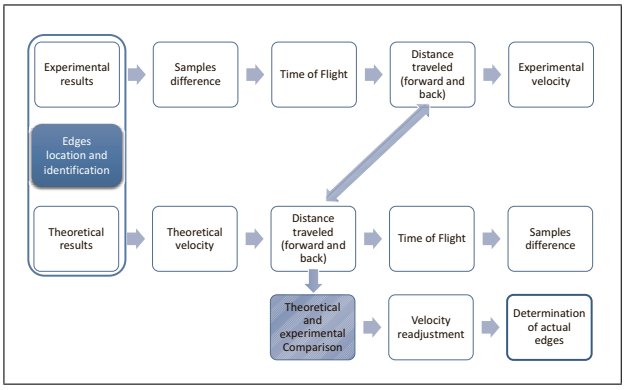

Figure 7. Theoretical and experimental comparison for edges identification.

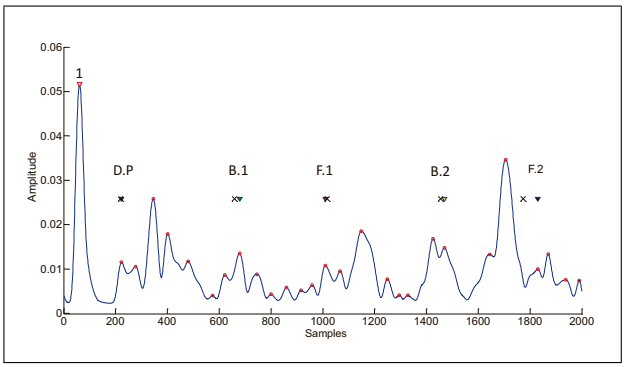

Figure 8. Edges reflections of L(0,2) mode by comparing the theoretical and experimental values of ToF.

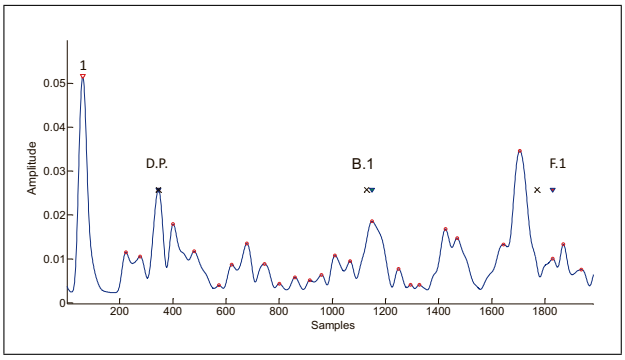

Figure 9. Edges reflections of L(0,1) mode by comparing the theoretical and experimental values of ToF.

6. The second reflection from the front edge (F.2).

Then, the $L(0, 1)$ mode is analysed analogously. The propagation velocity of this mode is 2807 m/s in this case. Figure 9 shows the edges reflection of the $L(0, 1)$ mode.

The peaks of both modes are discarded (Figure 8 and Figure 9). The rest of the echoes are considered as possible failures and they are analysed in detail.

4.4. Crack location

The longitudinal Lamb mode $L(0, 2)$ is studied to obtain the location of the damage. This mode is more sensitive to the changes in this case study.

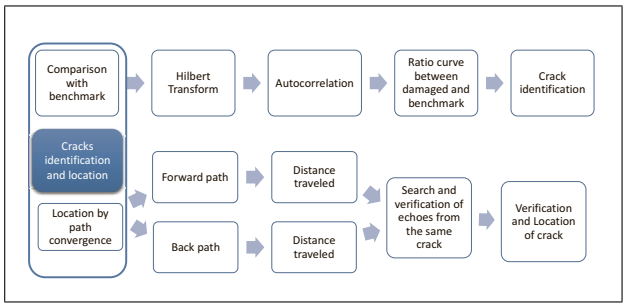

Figure 10. Location of the crack by two methods: comparison with the reference signal and location by convergence of different paths.

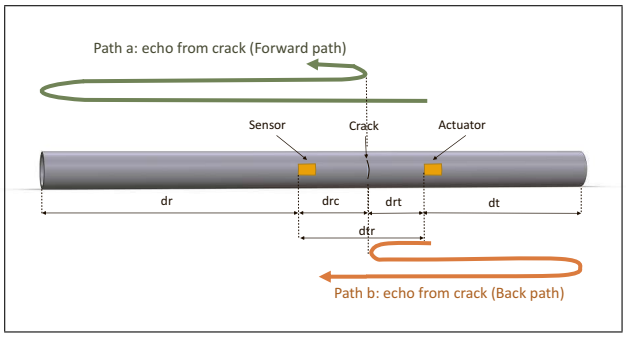

Figure 11. Two shortest paths from actuator to sensor detecting the crack.

The peaks that have not been considered yet are possible echoes that can come from a crack (X_{cracks}). The reflection from the crack could be overlaid with echoes from edges. The method does not consider these cases.

$$\boldsymbol{X}_{\text{cracks}} \subseteq \boldsymbol{X} : \boldsymbol{X}_{\text{cracks}} \notin \boldsymbol{X} \cap \boldsymbol{X}_{\text{edges}}. \tag{4}$$

The heights of $\boldsymbol{X}_{\text{cracks}}$ are

$$\begin{aligned} \boldsymbol{X}_{\text{cracks}} &= \left[X_{\text{cracks}_1}, \ldots, X_{\text{cracks}_k}, \ldots, X_{\text{cracks}_{n-m}}\right], \\ & \quad k = 1, 2, \ldots, n-m. \\ \boldsymbol{Y}_{\text{cracks}} &= \left[Y_{\text{cracks}_1}, \ldots, Y_{\text{cracks}_k}, \ldots, Y_{\text{cracks}_{n-m}}\right], \\ & \quad k = 1, 2, \ldots, n-m. \end{aligned}$$

The approach is based on the search for two echoes that come from the same crack, but have different routes. It considers that if the ToF employed to traverse a common section is almost equal, the defect is detected and therefore located. The scheme of this methodology is shown in Figure 10.

The two shortest paths for detecting a crack between the sensor and transmitter are shown as "a" and "b" in Figure 11. The distance travelled by an echo in "a", e.g. d_{echo_a}, is used to determine the distance drc_a between the crack and the receptor. The distance travelled by an echo in "b", d_{echo_b}, is employed to set the distance drc_b. The distances drc_a and drc_b should be the same. The method performs a comparison between the distances obtained for each component of X_{cracks}.

The paths are shown in Figure 11.

Path "a":

$$\begin{aligned} d_{\text{echo}_{a,k}} &= dtr + 2dr + 2drc_{a,k}, && (5) \\ drc_{a,k} &= \left(d_{\text{echo}_{a,k}} - dtr - 2dr\right)/2, && (6) \\ Drc_a &= \left[drc_{a,1}, \ldots, drc_{a,k}, \ldots, drc_{a,m-n}\right], \\ & \quad k = 1, 2, \ldots, n-m. \end{aligned}$$

Path "b":

$$\begin{aligned} d_{\text{echo}_{b,k}} &= 3dtc + 2dt + drc_{b,k}, && (7) \\ dtc &= dtr - drc_{b,k}, && (8) \\ d_{\text{echo}_{b,k}} &= 3\left(dtr - drc_{b,k}\right) + 2dt + drc, && (9) \\ drc_{b,k} &= \left(3dtr + 2dt - d_{\text{echo}_{b,k}}\right)/2, && (10) \\ Drc_b &= \left[drc_{b,1}, \ldots, drc_{b,k}, \ldots, drc_{b,m-n}\right], \\ & \quad k = 1, 2, \ldots, n-m. \end{aligned}$$

The distance $drc_{a,k}$ is compared with all the echoes that come from the path "b" ($drc_{b,k}$). The pair of echoes that provide the most similar distances, drc_1 and drc_2, have the greatest likelihood to come from the same notch.

$$\boldsymbol{D} = \begin{bmatrix} \left|drc_{a,1} - drc_{b,1}\right| & \cdots & \left|drc_{a,1} - drc_{b,l}\right| & \cdots \\ \vdots & & \vdots & \\ \left|drc_{a,k} - drc_{b,1}\right| & \cdots & \left|drc_{a,k} - drc_{b,l}\right| & \cdots \\ \vdots & & \vdots & \\ \left|drc_{a,n-m} - drc_{b,1}\right| & \cdots & \left|drc_{a,n-m} - drc_{b,l}\right| & \cdots \end{bmatrix} \begin{matrix} \cdots \left|drc_{a,1} - drc_{b,n-m}\right| \\ \vdots \\ \cdots \left|drc_{a,k} - drc_{b,n-m}\right| \\ \vdots \\ \cdots \left|drc_{a,n-m} - drc_{b,n-m}\right| \end{matrix}, \tag{11}$$

where $k = 1, 2, \ldots, n-m$ and $l = 1, 2, \ldots, n-m$. The signals could appear as superposition of two echoes that came from "a" and "b", i. e. they could be showed as a single peak. The main diagonal of $\boldsymbol{D}$ provides the solution for these cases. The component is the minimum difference between both paths, given by

$$e_{\text{crack},k,l} = d_{kl} : \; d_{kl} = \min\left(\boldsymbol{D}\right) \leftrightarrow d_{kl} < \tau, \; \forall k, l, \tag{12}$$

where τ is the tolerance. The distance of the crack from the sensor $f_{\text{crack},a}$ is given by

$$\begin{aligned} f_{\text{crack},a} &= drc_{a,k}, \forall k : \; d_{kl} = \min\left(\boldsymbol{D}\right) \\ & \leftrightarrow d_{kl} < \tau, \; \forall k, l. \end{aligned} \tag{13}$$

The main diagonal is not considered, i. e. it is assumed that there are no overlapping echoes. The difference between the $d_{rc_{a,k}}$ and $d_{rc_{b,l}}$ must be within the tolerance.

$$\begin{aligned} e_{\text{crack}} &= d_{kl} : \; d_{kl} = \min\left(\boldsymbol{D}\right) : k \neq l \\ & \leftrightarrow \boldsymbol{D}_{kl} < \tau, \; \forall k, l, && (14) \\ f_{\text{crack},a} &= drc_{a,k}, \forall k : \; d_{kl} = \min\left(\boldsymbol{D}\right) k \neq l \\ & \leftrightarrow d_{kl} < \tau, \; \forall k, l. && (15) \end{aligned}$$

Table II. Predicted notch by comparison of ratio curve with benchmark. Cut: Depth of the cut (mm); HP: Highest Point; TN: Tested notch (%); PN: Predicted notch (%); Error (%).

Cut	HP	TN	PN	Error
0.50	1.30	16	10	6
1.00	1.45	33	23	10
1.50	1.59	49	38	11
2.00	1.83	66	58	8
2.50	1.96	82	77	5
3.05	2.09	100	100	0

Theoretically, an echo coming from a crack should have a greater amplitude than the other echoes. The following equation weights the more similar distances with the amplitude of the two echoes of each path

$$f^{w}_{\text{crack},a} = drc_{a,k}, \forall k : \\ d_{kl} = \min\left(\frac{|d_{rc_{a,k}} - d_{rc_{b,l}}|}{y_{\text{cracks}_k} + y_{\text{cracks}_l}}\right) : \\ k \neq l,\ \forall k, l. \tag{16}$$

In many cases, the amplitude of the echoes is several orders of magnitude smaller than the "x" axis. The following heuristic method is employed to weight the amplitude and corrects this problem.

$$f^{w}_{\text{crack},a} = drc_{a,k}, \forall k : \\ d_{kl} = \min\left(\frac{\sqrt[g]{|d_{rc_{a,k}} - d_{rc_{b,l}}|}}{(y_{\text{cracks}_k} + y_{\text{cracks}_l})^{g}}\right) : \\ k \neq l,\ \forall k, l, g,\ g = 1, 2, 3, \ldots. \tag{17}$$

Figure 12 shows the echo coming from the crack by path "a". Similarly, the crack location it would be the same if path "b" had been chosen.

Finally, when the location is determined, the crack is shown in a schema with the dimensions of the plate and the position of the sensors (Figure 13).

Note that the roll of the transducers can be inversed. The method shown is consistent for the role exchange. In that case, in the input data, the values of *dr* and *dt* must be exchanged with the values of *drc* and *drt* respectively.

4.5. Notch sizing

The correction method explained in section B is employed to obtain the notch size. The ratio curve is obtained by dividing each autocorrelation with the autocorrelation of the reference signal. Figure 14 shows the ratio curves and the behaviour of the curves when the echo coming from the damage is collected. The amplitude variations of the curves are proportional to the notch.

The predicted notch is obtained using the equation

$$Predicted_{dmge_i} = \\ \frac{Highest_{point_i} \cdot Tested_{dmge_i} \cdot Predicted_{dmge_i}}{Highest_{point_n} \cdot Tested_{dmge_n}}, \\ i = 1, 2, \ldots, n. \tag{18}$$

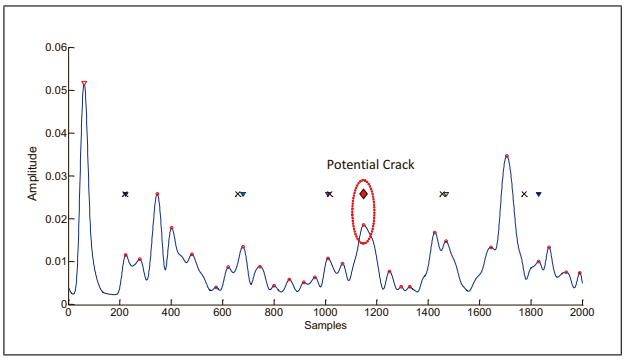

Figure 12. Echo coming from the crack via path a.

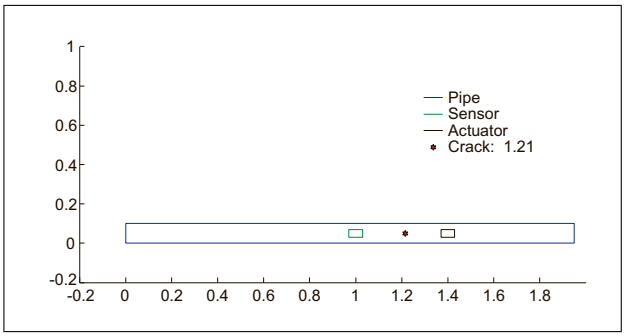

Figure 13. Crack location relative to the left edge in meters.

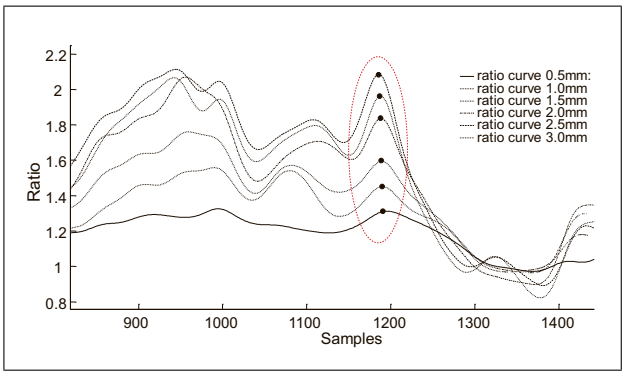

Figure 14. Ratio curve between the autocorrelations of each signal with the benchmark signal.

The ratio curve is computed by dividing the autocorrelation curve of the damage signal by the autocorrelation of the reference signal. The highest point in each ratio curve is called *Highest_point*. The *Tested_dmge* is the ratio of depth of the cut by the thickness of the pipe (3.05 mm). The predicted notch (*Predicted_dmge*) is the proportional expected percentage of notch depth computed by taking the highest Ratio Point (1. 3) divided by the highest base point (2.09) and multiplied by 16%. The error is the difference between the tested notch and predicted notch.

Lamb waves propagation in tubes of 316L material is not considered in this paper because there are studies that consider it as [64] and [65]. The method has been tested in the short distances scenarios considered in this paper, and it should be tested for other cases studies.

5. Conclusions

A new advanced signal processing approach for cylindrical Lamb waves has been developed. The method provides more precise information about the structural state of the pipe, that leads to an increase in safety, reliability availability and investing returns. This work presents a novel approach based on signal processing to automatically identify, locate and determine the severity of a notch in a pipe under certain conditions. The approach combines two different techniques: The first identifies the time of flight of both longitudinal Lamb modes, used to automatically identify the edges or welds of the pipes. Time of flight of the echoes are calculated theoretically and then compared with the experimental times to determine that echoes come from the edges; the second technique uses the correction method in order to identify the differences between the signals in the cases with notches and the reference signals. Then, the position in the time domain of these differences is compared with t he echoes obtained in the first technique, where the location of the notch is obtained. Echoes from the same notch traveling different paths are compared and the defect is located considering each amplitude. The second technique allows knowing the severity of the notch by analysing the changes in the ratio curve between the autocorrelations of the different signals. The method has been validated for short distances.

Acknowledgements

The work reported herewith has been financially partially supported by the Spanish Ministerio de Economía y Competitividad, under Research Grant DPI2015-67264-P.

References

[1] F. P. G. Márquez, J. M. C. Muñoz: A pattern recognition and data analysis method for maintenance management. International Journal of Systems Science **43** (2012) 1014–1028.

[2] F. P. G. Marquez: An approach to remote condition monitoring systems management. International Conference on Railway Condition Monitoring. The Institution of Engineering and Technology IET, 2006, 156–160.

[3] A. Light-Marquez, A. Sobin, G. Park, K. Farinholt: Structural damage identification in wind turbine blades using piezoelectric active sensing.in structural dynamics and renewable energy. Volume 1. Springer, 2011, 55–65.

[4] F. P. G. Márquez, A. M. Tobias, J. M. P. Pérez, M. Papaelias: Condition monitoring of wind turbines: Techniques and methods. Renewable Energy **46** (2012) 169–178.

[5] K. Papakonstantinou, M. Shinozuka: Planning structural inspection and maintenance policies via dynamic programming and markov processes. Part I: Theory. Reliability Engineering & System Safety **130** (2014) 202–213.

[6] A. Van Horenbeek, L. Pintelon: Development of a maintenance performance measurement framework using the analytic network process (anp) for maintenance performance indicator selection. Omega **42** (2014) 33–46.

[7] K.-A. Nguyen, P. Do, A. Grall: Multi-level predictive maintenance for multi-component systems. Reliability Engineering & System Safety **144** (2015) 83–94.

[8] F. Marquez: Binary decision diagrams applied to fault tree analysis [c]. 4th LET International Conference on Railway Condition Monitoring, 2008, 126–128.

[9] F. P. García, D. J. Pedregal, C. Roberts: Time series methods applied to failure prediction and detection. Reliability Engineering & System Safety **95** (2010) 698–703.

[10] D. J. Pedregal, F. P. García, C. Roberts: An algorithmic approach for maintenance management based on advanced state space systems and harmonic regressions. Annals of Operations Research **166** (2009) 109–124.

[11] M. Papaelias, F. G. Márquez, J. C. Muñoz, C. Roberts: A b-spline approach to alternating current field measurement for railroad inspection. IEEE International Conference on Industrial Engineering and Engineering Management, 2008, 1385–1389.

[12] F. P. G. Márquez: A new method for maintenance management employing principal component analysis. Structural Durability & Health Monitoring **6** (2010) 89–99.

[13] C. Gomez Munoz, R. De la Hermosa Gonzalez-Carrato, J. Trapero Arenas, F. Garcia Marquez: A novel approach to fault detection and diagnosis on wind turbines. Global Nest Journal **16** (2014) 1029–1037.

[14] J. Edwards: Signal processing opens new views on imaging [special reports]. IEEE Signal Processing Magazine **32** (2015) 8–18.

[15] C. Q. Gómez Muñoz, F. P. García Márquez: A new fault location approach for acoustic emission techniques in wind turbines. Energies **9** (2016) 40.

[16] G. anzano, E. Salzano, F. S. de Magistris, G. Fabbrocino: Seismic vulnerability of natural gas pipelines. Reliability Engineering & System Safety **117** (2013) 73–80.

[17] W. J. Gomes, A. T. Beck, T. Haukaas: Optimal inspection planning for onshore pipelines subject to external corrosion. Reliability Engineering & System Safety **118** (2013) 18–27.

[18] D. Dai, Q. He: Structure damage localization with ultrasonic guided waves based on a time–frequency method. Signal Processing **96** (2014) 21–28.

[19] F. M. Favarò, D. W. Jackson, J. H. Saleh, D. N. Mavris: Software contributions to aircraft adverse events: Case studies and analyses of recurrent accident patterns and failure mechanisms. Reliability Engineering & System Safety **113** (2013) 131–142.

[20] S. Zhang, W. Zhou: Bayesian dynamic linear model for growth of corrosion defects on energy pipelines. Reliability Engineering & System Safety **128** (2014) 24–31.

[21] C.-T. Ng: Bayesian model updating approach for experimental identification of damage in beams using guided waves. Structural Health Monitoring **13** (2014) 359–373.

[22] C. M. Yeum, H. Sohn, H. J. Lim, J. B. Ihn: Reference-free delamination detection using Lamb waves. Structural Control and Health Monitoring **21** (2014) 675–684.

[23] L. Ge, X. Wang, C. Jin: Numerical modeling of pzt-induced Lamb wave-based crack detection in plate-like structures. Wave Motion **51** (2014) 867–885.

[24] Z. Tian, C. Leckey, M. Rogge, L. Yu: Crack detection with Lamb wave wavenumber analysis. SPIE Smart Structures and Materials + Nondestructive Evaluation and Health Monitoring, International Society for Optics and Photonics, 2013, 86952Z–86952Z–86913.

[25] Y. Yao, S. T. E. Tung, B. Glisic: Crack detection and characterization techniques – an overview. Structural Control and Health Monitoring **21** (2014) 1387–1413.

[26] Z. Su, L. Ye, Y. Lu: Guided Lamb waves for identification of damage in composite structures: A review. Journal of Sound and Vibration **295** (2006) 753–780.

[27] M. J. Lowe, D. N. Alleyne, P. Cawley: Defect detection in pipes using guided waves. Ultrasonics **36** (1998) 147–154.

[28] C. Q. G. Muñoz, F. P. G. Márquez, J. M. S. Tomás: Ice detection using thermal infrared radiometry on wind turbine blades. Measurement **93** (2016) 157–163.

[29] J. L. Rose: Recent advances in guided wave nde. Proceedings Ultrasonics Symposium, 1995, 761–770.

[30] J. L. Rose: A baseline and vision of ultrasonic guided wave inspection potential. Journal of Pressure Vessel Technology **124** (2002) 273–282.

[31] N. Krautkramer: Emerging technology – guided wave ultrasonics. NDTnet, June 1998.

[32] D. Alleyne, B. Pavlakovic, M. Lowe, P. Cawley: Rapid, long range inspection of chemical plant pipework using guided waves. – In: Review of Progress in Quantitative Nondestructive Evaluation: Volume 20. AIP Publishing, 2001, 180–187.

[33] D. Thomson, D. Chimenti: Review of progress in quantitative nondestructive evaluation. Chapter 2c "guided waves" and Chapter 7 "nde applications". AIP Conference Proceedings, 2002.

[34] G. Nie, J. Liu, X. Liu: Lamb wave propagation in a piezoelectric/piezomagnetic bi-material plate with an imperfect interface. Acta Acustica united with Acustica **102** (2016) 893–901.

[35] J.-L. Christen, M. Ichchou, A. Zine, B. Troclet: Wave finite element formulation of the acoustic transmission through complex infinite plates. Acta Acustica united with Acustica **102** (2016) 984–991.

[36] A. Bagheri, K. Li, P. Rizzo: Reference-free damage detection by means of wavelet transform and empirical mode decomposition applied to Lamb waves. Journal of Intelligent Material Systems and Structures **24** (2013) 194–208.

[37] P. Aryan, A. Kotousov, C. T. Ng, B. Cazzolato: A model-based method for damage detection with guided waves. Structural Control and Health Monitoring **24** (2017).

[38] H. Lamb: On waves in an elastic plate. Proceedings of the Royal Society of London A: Mathematical, Physical and Engineering Sciences (1917) 114–128.

[39] D. N. Alleyne, P. Cawley: Optimization of Lamb wave inspection techniques. Ndt & E International **25** (1992) 11–22.

[40] M. Silk, K. Bainton: The propagation in metal tubing of ultrasonic wave modes equivalent to Lamb waves. Ultrasonics **17** (1979) 11–19.

[41] D. C. Gazis: Three-dimensional investigation of the propagation of waves in hollow circular cylinders.i.analytical foundation. The Journal of the Acoustical Society of America **31** (1959) 568–573.

[42] D. C. Gazis: Three-dimensional investigation of the propagation of waves in hollow circular cylinders.ii.numerical results. The Journal of the Acoustical Society of America **31** (1959) 573–578.

[43] A. H. Fitch: Observation of elastic-pulse propagation in axially symmetric and nonaxially symmetric longitudinal modes of hollow cylinders. The Journal of the Acoustical Society of America **35** (1963) 706–708.

[44] J. Ditri, J. Rose, F. Carr, W. McKnight: A novel guided ultrasonic wave technique for improved tubing inspection efficiency. 11 th International Conference on NDE in the Nuclear and Pressure Vessel Industries, 1992, 49–54.

[45] J. J. Ditri, J. L. Rose, G. Chen: Mode selection criteria for defect detection optimization using Lamb waves. Review of Progress in Quantitative Nondestructive Evaluation. Vol.11B (1992) 2109–2115.

[46] P. Tua, S. Quek, Q. Wang: Detection of cracks in cylindrical pipes and plates using piezo-actuated Lamb waves. Smart materials and structures **14** (2005) 1325.

[47] P. Tua, S. Quek, Q. Wang: Detection of cracks in plates using piezo-actuated Lamb waves. Smart Materials and Structures **13** (2004) 643.

[48] F. L. Discalea, H. Matt, I. Bartoli, S. Coccia, G. Park, C. Farrar: Health monitoring of uav wing skin-to-spar joints using guided waves and macro fiber composite transducers. Journal of intelligent material systems and structures **18** (2007) 373–388.

[49] A. Raghavan, C. E. Cesnik: Review of guided-wave structural health monitoring. Shock and Vibration Digest **39** (2007) 91–116.

[50] A. A. Jiménez, C. Q. G. Muñoz, F. P. G. Marquez, L. Zhang: Artificial intelligence for concentrated solar plant maintenance management. – In: Proceedings of the Tenth International Conference on Management Science and Engineering Management. Springer, 2017, 125–134.

[51] K. Diamanti, C. Soutis, J. Hodgkinson: Lamb waves for the non-destructive inspection of monolithic and sandwich composite beams. Composites Part A: Applied science and manufacturing **36** (2005) 189–195.

[52] Z. Su, L. Ye: Identification of damage using Lamb waves: From fundamentals to applications. Springer Science & Business Media **48** (2009).

[53] P. Wilcox, M. Lowe, P. Cawley: Mode and transducer selection for long range Lamb wave inspection. Journal of intelligent material systems and structures **12** (2001) 553–565.

[54] X. Wang, W. T. Peter, C. K. Mechefske, M. Hua: Experimental investigation of reflection in guided wave-based inspection for the characterization of pipeline defects. NDT & E International **43** (2010) 365–374.

[55] P. Cawley, M. Lowe, D. Alleyne, B. Pavlakovic, P. Wilcox: Practical long range guided wave inspection-applications to pipes and rail. Materials evaluation **61** (2003) 66–74.

[56] M. Papaelias, L. Cheng, M. Kogia, A. Mohimi, V. Kappatos, C. Selcuk, L. Constantinou, C. Q. G. Muñoz, F. P. G. Marquez, T.-H. Gan: Inspection and structural health monitoring techniques for concentrated solar power plants. Renewable Energy **85** (2016) 1178–1191.

[57] P. Coverley, W. Staszewski: Impact damage location in composite structures using optimized sensor triangulation procedure. Smart materials and structures **12** (2003) 795.

[58] F. P. García Márquez, I. P. García-Pardo: Principal component analysis applied to filtered signals for maintenance management. Quality and Reliability Engineering International **26** (2010) 523–527.

[59] C. Q. G. Muñoz, A. A. Jiménez, F. P. G. Márquez: Wavelet transforms and pattern recognition on ultrasonic guides waves for frozen surface state diagnosis. Renewable Energy (2017).

[60] X. Zhao, H. Gao, G. Zhang, B. Ayhan, F. Yan, C. Kwan, J. L. Rose: Active health monitoring of an aircraft wing with embedded piezoelectric sensor/actuator network. I: Defect detection, localization and growth monitoring. Smart materials and structures **16** (2007) 1208.

[61] S. Hurlebaus, M. Niethammer, L. J. Jacobs, C. Valle: Automated methodology to locate notches with Lamb waves. Acoustics Research Letters Online **2** (2001) 97–102.

[62] M. Kadzi?ski, T. Tervonen, J. R. Figueira: Robust multi-criteria sorting with the outranking preference model and characteristic profiles. Omega **55** (2015) 126–140.

[63] S. Mattar, R. Macdonald, E. Choo: Procurement process: Decision by exclusion and pairwise comparisons. Omega **20** (1992) 705–712.

[64] K. I. Lee, S. W. Yoon: Propagation of time-reversed Lamb waves in acrylic cylindrical tubes as cortical-bone-mimicking phantoms. Applied Acoustics **112** (2016) 10–13.

[65] B. Wu, Y. Su, W. Chen, C. Zhang: On guided circumferential waves in soft electroactive tubes under radially inhomogeneous biasing fields. Journal of the Mechanics and Physics of Solids **99** (2017) 116–145.